Effect of interfacial adhesion on the ultrasonic interaction with adhesive joints: A theoretical study using spring-type interfaces

Naoki Mori,[1,a)] Naoki Matsuda,[2] and Takayuki Kusaka[1]
[1]*Department of Mechanical Engineering, Ritsumeikan University, 1-1-1 Noji-higashi, Kusatsu, Shiga 525-8577, Japan*
[2]*Department of Mechanical Engineering and Science, Kyoto University, Katsura, Nishikyo-ku, Kyoto 615-8540, Japan*

(Received 24 February 2019; revised 20 May 2019; accepted 29 May 2019; published online 18 June 2019)

The effect of interfacial properties on the reflection and transmission characteristics of ultrasonic waves at adhesively bonded joints is theoretically investigated. An adhesive joint is modeled as a double-interface model, namely, a homogeneous layer coupled to adherends by two spring-type interfaces with different interfacial stiffnesses. For the normal incidence of a one-dimensional longitudinal wave, theoretical results are obtained and validated by finite element simulation. When the thickness of the adhesive layer is sufficiently small compared to the wavelength, the amplitude reflection and transmission coefficients show monotonic dependence on frequency, which can be explained by the theoretical relation of the double-interface model to a single spring-type interface model. The reflection and transmission behavior is invariant if the values of the two interfacial stiffnesses are interchanged. For a relatively thick adhesive layer, on the other hand, the reflection coefficient shows local minima at multiple frequencies. As one interfacial stiffness decreases, the local minimum frequencies decrease and the local minima increase. If the values of the two interfacial stiffnesses are interchanged, the reflection coefficient remains invariant but the reflection waveform shows different features. The obtained reflection and transmission characteristics are discussed in light of the characterization of the interfacial adhesion.
https://doi.org/10.1121/1.5111856

[KML] Pages: 3541–3550

I. INTRODUCTION

Adhesive joining technology has been developing in terms of material and mechanical sciences in recent years. As the adhesive joining gains popularity in various industries, such as aircraft and automobiles, the nondestructive evaluation (NDE) for adhesively bonded joints becomes more indispensable. Among various NDE methods for adhesive joints, ultrasonic waves play an important role not only in the detection of defects including voids and cracks but also in the characterization of the bond thickness, the cohesive properties such as elastic or viscoelastic moduli, and the adhesive properties (the properties of adherend−adhesive interfaces).[1–4]

In the characterization of adhesive joints by ultrasonic waves, the modeling of the joint is essential to interpret the measured data precisely. Various models were proposed in previous studies, and the model parameters were identified from the measured results of reflected or transmitted waves from adhesive joints. In most cases, an adhesive joint is modeled as a tri-layer structure, which has an adhesive layer sandwiched between two adherends,[4–15] and the continuity condition is imposed on the displacement and stress components at the adherend–adhesive interfaces. The effect of cohesive properties on the ultrasonic behavior can be examined in this model, which is referred to as the interlayer model in the present study. When modeling adhesive joints for the numerical simulation by finite element method (FEM) or finite-difference method (FDM), however, the discretization of adhesive layers sometimes leads to high computational cost because fine meshes are required to accurately express the wave propagation in thin layers. Thus a single-interface model is used as a convenient model for adhesive joints, in which an adhesive layer is replaced by equivalent distributed springs.[8,9,16–22] When the thickness of the adhesive layer is sufficiently thin compared to the wavelength, the interlayer model can be reproduced by the single-interface model with the interfacial stiffnesses expressed by the cohesive properties. In general, the interfacial stiffnesses in the single-interface model depend on both cohesive and adhesive properties of bonded joints.

In order to consider cohesive and adhesive properties separately, a double-interface model is often used in previous studies.[23–34] An adhesive joint is modeled as a tri-layer structure analogously to the interlayer model, but two adherend–adhesive interfaces are modeled by spring-type interfaces. Each spring-type interface reflects a thin interphase region between an adherend and an adhesive layer. The double-interface model is also used for the modeling of a plate compressed by two blocks because the spring-type interface model can be applied to contacting surfaces between solids.[19,21,35–38] For a thin aluminum plate compressed by two aluminum blocks, Lavrentyev and Rokhlin[35] derived the reflection coefficient in the double-interface

a)Electronic mail: nmori@fc.ritsumei.ac.jp

model, which was used to discuss the measured reflection spectra at the contacting surfaces. Their concept was extended by Baltazar *et al.*[28] for the estimation of the cohesive and adhesive properties of environmentally degraded adhesive joints using reflection spectra. In these studies, however, the interfacial stiffnesses of the two interfaces were assumed to be identical. For adhesively bonded joints, one of the adherend−adhesive interfaces could be degraded with the other maintaining integrity due to improper adherend surface treatment before bonding, such as adherend contamination by chemicals. It is therefore of importance to investigate the effect of the two different interfaces on the reflection and transmission behavior. However, to the authors' knowledge, this topic has not sufficiently been explored.[26,27]

The aim of the present study is to reveal the effect of the interfacial adhesion on the reflection and transmission characteristics of ultrasonic waves at an adhesive joint. In particular, the reflection and transmission behavior in the double-interface model with different interfacial properties is theoretically examined. A one-dimensional theoretical analysis is performed to derive the reflection and transmission coefficients, which are shown for two cases: (I) when the adhesive layer is sufficiently thin compared to the wavelength and (II) when the adhesive layer thickness is comparable to the wavelength. Some previous papers considered three-dimensional problems regarding an interface between two dissimilar materials,[39,40] but the present study deals with one-dimensional wave propagation for simplicity. The obtained reflection and transmission characteristics are discussed by comparing to the results of the single-interface model.

This paper is structured as follows. In Sec. II, three different models for adhesive joints, namely, the interlayer model, the single-interface model, and the double-interface model are briefly described. In Sec. III, the reflection and transmission characteristics for the normal incidence of the one-dimensional wave are theoretically obtained for the double-interface model. To validate the theoretical results, a finite element simulation is performed in Sec. IV. In Sec. V, the reflection and transmission characteristics in the double-interface model are further explored using the theoretical results and the transient responses obtained by FEM.

II. THEORETICAL MODELS FOR ADHESIVE JOINTS

In this study, an adhesive joint subjected to the normal wave incidence shown in Fig. 1(a) is modeled in three different manners, as shown in Figs. 1(b)–1(d). For simplicity, the normal incidence of a one-dimensional longitudinal wave to the adhesive joint is considered in all models. The adherends are semi-infinite, homogeneous, and linear elastic bodies. The propagation direction of the incident wave is set as x axis. The wave propagation in the adherends obeys the wave equation

$$\frac{\partial^2 u}{\partial t^2} = \frac{1}{\rho}\frac{\partial \sigma}{\partial x} = \frac{1}{\rho}\frac{\partial}{\partial x}\left(\rho c^2 \frac{\partial u}{\partial x}\right) = c^2 \frac{\partial^2 u}{\partial x^2}, \tag{1}$$

where t is time, ρ and c are the mass density and the wave velocity of the adherends, $u = u(x, t)$ is the displacement component, and $\sigma = \sigma(x, t)$ is the stress component. In Eq. (1), Hooke's law is applied in order to relate the displacement and stress components.

Figure 1(b) corresponds to the interlayer model, which is widely used for the modeling of adhesive joints in the ultrasonic reflection and transmission analysis.[4–15] The adhesive layer is replaced by a homogeneous layer of thickness h in $0 < x < h$, which is modeled as elastic or viscoelastic material. The continuity condition of the displacement and stress components is applied at two adherend−adhesive interfaces $x = 0$ and $x = h$, namely,

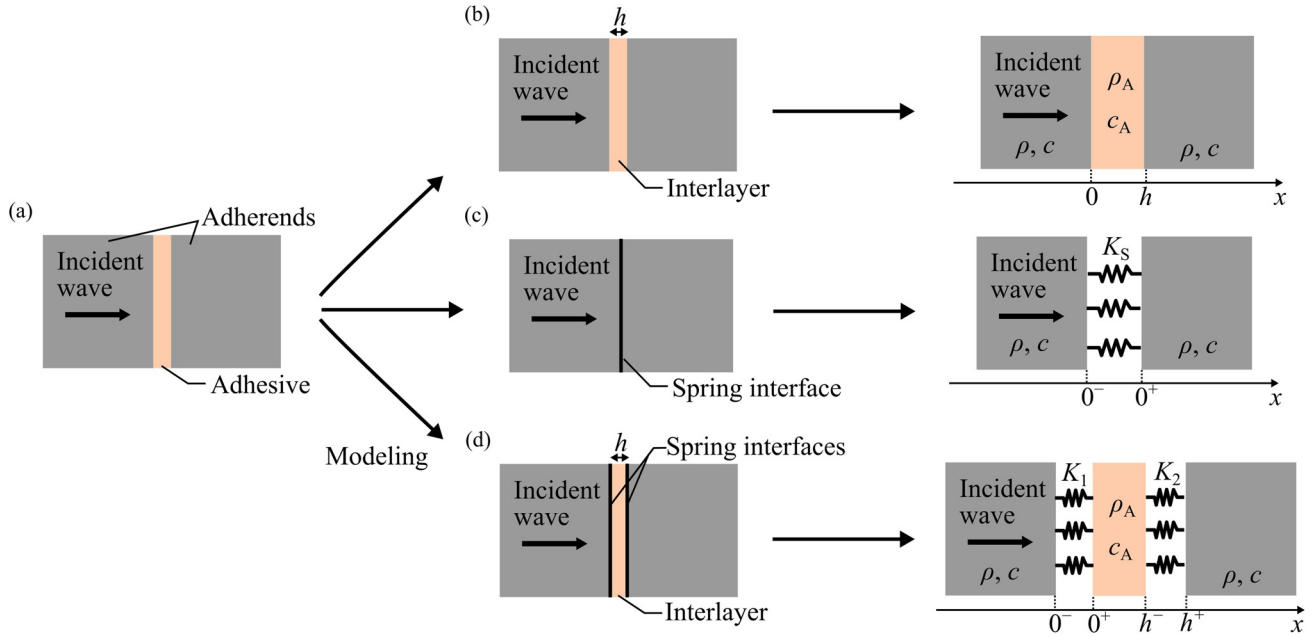

FIG. 1. (Color online) Schematics of (a) an adhesive joint subjected to the normal wave incidence, and three different models for the ultrasonic reflection and transmission analysis: (b) the interlayer model, (c) the single-interface model, and (d) the double-interface model.

$$u(0^+,t)=u(0^-,t),\quad \sigma(0^+,t)=\sigma(0^-,t),$$
$$u(h^+,t)=u(h^-,t),\quad \sigma(h^+,t)=\sigma(h^-,t), \tag{2}$$

where the superscript + (−) represents the right (left) side of the interface, i.e., $u(0^{\pm},t)=\lim_{x\to\pm 0}u(x,t)$, for instance. In this study, the adhesive layer is modeled by linear elastic material of the wave velocity c_A and the mass density ρ_A, and its viscosity is not considered for simplicity.

Figure 1(c) shows the single-interface model, which can be used for a thin adhesive layer.[16–22] The adhesive layer is replaced by equivalent springs distributed along the joint surfaces. When the interface is located at $x=0$, the boundary condition is expressed as

$$\sigma(0^+,t)=\sigma(0^-,t)=K_S\left[u(0^+,t)-u(0^-,t)\right], \tag{3}$$

where K_S is the interfacial stiffness. The stress component is continuous at the joint, while the displacement component can be discontinuous. This spring-type interface model is also used for the modeling of contacting surfaces between solids[35–38] and damaged interfaces.[41]

Figure 1(d) corresponds to the double-interface model,[23–34] which is analogous to the interlayer model shown in Fig. 1(b). The adhesive layer is similarly modeled as a homogeneous layer of thickness h in $0<x<h$, but the boundary condition of spring-type interfaces is applied to the adherend–adhesive interfaces at $x=0$ and $x=h$ instead of Eq. (2), i.e.,

$$\sigma(0^+,t)=\sigma(0^-,t)=K_1\left[u(0^+,t)-u(0^-,t)\right],$$
$$\sigma(h^+,t)=\sigma(h^-,t)=K_2\left[u(h^+,t)-u(h^-,t)\right], \tag{4}$$

where K_1 and K_2 represent the interfacial stiffnesses of the interfaces at $x=0$ and $x=h$, respectively. When K_1 and K_2 approach infinity, the double-interface model is reduced to the interlayer model.

III. THEORETICAL REFLECTION AND TRANSMISSION CHARACTERISTICS

For the single-interface model and the double-interface model in Sec. II, the normal incidence of a harmonic longitudinal wave is considered. For the single-interface model in Fig. 1(c), the displacement field in the adherends is written as

$$u=\exp(\mathrm{i}\omega x/c)+R\exp(-\mathrm{i}\omega x/c),\quad x<0,$$
$$u=T\exp(\mathrm{i}\omega x/c),\quad x>0, \tag{5}$$

where $\mathrm{i}=\sqrt{-1}$, $\omega=2\pi f$ is angular frequency, and R and T are reflection and transmission coefficients. The time-dependent term $\exp(-\mathrm{i}\omega t)$ is omitted from all terms in Eq. (5). Substitution of Eq. (5) into Eq. (3) leads to

$$R=\frac{\mathrm{i}\Omega_S}{\mathrm{i}\Omega_S-2},\quad T=-\frac{2}{\mathrm{i}\Omega_S-2}, \tag{6}$$

which are determined only by the non-dimensional quantity $\Omega_S=\rho c\omega/K_S$, as obtained in previous papers.[17–22] In particular, the amplitude reflection coefficient $|R|$ increases monotonically with increasing Ω_S. As reported in previous studies, the interfacial stiffness K_S can be estimated by

$$K_S=\frac{\rho c\omega}{2|R|}\sqrt{1-|R|^2}, \tag{7}$$

from the measured value of the amplitude reflection coefficient $|R|$ at angular frequency ω.

Likewise, for the double-interface model in Fig. 1(d), the displacement field in the tri-layer structure is written as

$$u=\exp(\mathrm{i}\omega x/c)+R\exp(-\mathrm{i}\omega x/c),\quad x<0,$$
$$u=A\exp(\mathrm{i}\omega x/c_A)+B\exp(-\mathrm{i}\omega x/c_A),\quad 0<x<h,$$
$$u=T\exp(\mathrm{i}\omega x/c),\quad x>h, \tag{8}$$

where R and T are reflection and transmission coefficients, and A and B are wave amplitudes in the adhesive layer. By substituting Eq. (8) into Eq. (4), a system of linear equations in the coefficients R, T, A, and B is obtained. The reflection coefficient R is derived as

$$R=\frac{-\mathrm{i}\frac{\Omega_1+\Omega_2}{2}\cos(k_Ah)-\frac{\mathrm{i}r}{2}\left(1+\mathrm{i}\frac{\Omega_2-\Omega_1}{r^2}-\frac{\Omega_1\Omega_2}{r^2}-\frac{1}{r^2}\right)\sin(k_Ah)}{\left(1-\mathrm{i}\frac{\Omega_1+\Omega_2}{2}\right)\cos(k_Ah)-\frac{\mathrm{i}r}{2}\left(1-\mathrm{i}\frac{\Omega_1+\Omega_2}{r^2}-\frac{\Omega_1\Omega_2}{r^2}+\frac{1}{r^2}\right)\sin(k_Ah)}, \tag{9}$$

where $k_A=\omega/c_A$ is the wavenumber in the adhesive, $r=\rho c/(\rho_Ac_A)$ is the acoustic impedance ratio, $\Omega_1=\rho c\omega/K_1$, and $\Omega_2=\rho c\omega/K_2$. The reflection coefficient in the case of $K_1=K_2$ was implicitly given by Lavrentyev and Rokhlin,[35] but to the authors' knowledge the general case of $K_1\neq K_2$ is shown here for the first time.

When the adhesive layer is sufficiently thin, i.e., $k_Ah=\omega h/c_A\ll\min(1,\ K_1/K_{AL},\ K_2/K_{AL})$, where $K_{AL}=\rho_Ac_A{}^2/h$, and the acoustic impedance of the adhesive is sufficiently lower than the adherends, i.e., $1/r=\rho_Ac_A/(\rho c)\ll 1$, the reflection coefficient of Eq. (9) can be simplified as

$$R \cong \frac{-\mathrm{i}\dfrac{\Omega_1+\Omega_2}{2}-\dfrac{\mathrm{i}r}{2}k_\mathrm{A}h}{1-\mathrm{i}\dfrac{\Omega_1+\Omega_2}{2}-\dfrac{\mathrm{i}r}{2}k_\mathrm{A}h}=\frac{\mathrm{i}(\Omega_1+\Omega_2+rk_\mathrm{A}h)}{\mathrm{i}(\Omega_1+\Omega_2+rk_\mathrm{A}h)-2}, \tag{10}$$

which corresponds to the formula for the single-interface model given in Eq. (6) with $\Omega_\mathrm{S}=\Omega_1+\Omega_2+rk_\mathrm{A}h$, namely,

$$\frac{1}{K_\mathrm{S}}=\frac{1}{K_1}+\frac{1}{K_2}+\frac{1}{K_\mathrm{AL}}, \tag{11}$$

which is an analogous form of the equivalent spring constant for springs in series. This result indicates that if the adhesive layer is sufficiently thin and has relatively low acoustic impedance, the double-interface model can be approximated by the single-interface model using Eq. (11). In the asymptotic case of $K_1 \to \infty$ and $K_2 \to \infty$, which corresponds to the interlayer model in Fig. 1(b), the interfacial stiffness K_S can be related to the cohesive properties by a well-known equation

$$K_\mathrm{S}=K_\mathrm{AL}=\frac{\rho_\mathrm{A}c_\mathrm{A}^2}{h}. \tag{12}$$

The relation of Eq. (11) shows that the interfacial compliance in the single-interface model $1/K_\mathrm{S}$ can be expressed as the sum of the cohesive property $1/K_\mathrm{AL}$ and the adhesive property $1/K_1+1/K_2$ in the double-interface model.

In this study, two cases are considered to examine the effect of the interfacial stiffnesses on the reflection and transmission behavior. In case I, the adhesive thickness is set to be sufficiently small compared to the wavelength, while a relatively thick adhesive layer is considered in case II.

IV. FINITE ELEMENT SIMULATION

A. Numerical model

To validate the theoretical results in Sec. III, two-dimensional numerical simulation by time-domain FEM is carried out for the double-interface model. As shown in Fig. 2, two homogeneous and linear elastic solids of thickness $L=50$ mm and width W are bonded by an adhesive layer of thickness h under the plane-strain condition. The spring-type boundary condition given in Eq. (4) is applied for the displacement and stress components at two adherend−adhesive interfaces. The periodic boundary condition is imposed on the upper and lower edges, and the normal traction is applied uniformly on the left edge to excite a

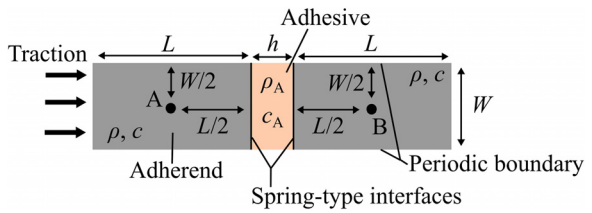

FIG. 2. (Color online) Numerical model of an adhesive joint for the finite element simulation.

longitudinal plane wave. Namely, the numerical model is two-dimensional but the wave propagation behavior is substantially one-dimensional. The displacement component in the horizontal direction is calculated at two points A and B, which are located $L/2$ away from the left and right adhesive interfaces, respectively. The waveforms of the incident and reflected waves are calculated at the point A, and the transmission waveform is obtained at the point B. The mass densities and the wave velocities are set as $\rho=2.7\times10^3\,\mathrm{kg/m^3}$ and $c=6.4$ km/s for the adherends, and $\rho_\mathrm{A}=1.2\times10^3\,\mathrm{kg/m^3}$ and $c_\mathrm{A}=2.0$ km/s for the adhesive, respectively. These parameters are based on the material properties of aluminum alloy and polymer-based adhesive. The acoustic impedance ratio is $r=\rho c/(\rho_\mathrm{A}c_\mathrm{A})=7.2$.

In accordance with cases I and II in the theoretical analysis, two different cases are considered in the finite element simulation. In case I, the adhesive thickness is set as $h=0.02$ [mm]. A Gaussian-modulated tone-burst

$$g(t)=\exp\left[-\left(\frac{t-t_0}{\sigma_0}\right)^2\right]\sin[2\pi f_0(t-t_0)], \tag{13}$$

is prescribed as the normal traction at the left edge, where $t_0=10\,\mu$s, $\sigma_0=1.5\,\mu$s, and $f_0=\omega_0/(2\pi)=0.5$ MHz is the center frequency. On this condition the non-dimensional quantity $\omega_0 h/c_\mathrm{A}$ becomes $\omega_0 h/c_\mathrm{A}=0.03$, which indicates that the adhesive layer is sufficiently small compared to the wavelength at the center frequency. In case II, on the other hand, the adhesive thickness is $h=0.2$ mm, and the center frequency of the input waveform is set as $f_0=\omega_0/(2\pi)=4$ MHz with $t_0=10\,\mu$s and $\sigma_0=0.2\,\mu$s. In this situation the non-dimensional quantity $\omega_0 h/c_\mathrm{A}$ is larger than unity, i.e., $\omega_0 h/c_\mathrm{A}=2.5$, which corresponds to a relatively thick adhesive layer compared to the wavelength.

The numerical models described above were discretized by four-node square-shaped isoparametric elements. Since the frequency ranges were different in cases I and II, elements with different sizes were used. For the modeling of the adhesive layers, the side lengths of the elements were 10 and $5\,\mu$m in cases I and II, which correspond to approximately 0.1% and 2% of the wavelength, respectively. Time integration was performed in an explicit scheme using the fourth-order Runge-Kutta method under the lumped mass matrix approximation. Time steps were set as 10 and $5\,\mu$s in cases I and II, respectively, to satisfy the stability condition.

B. Verification of the theoretical results

The waveforms at the two points A and B are obtained by FEM for $K_1=K_2=1$ MPa/nm, and the calculated results for cases I and II are shown in Figs. 3(a) and 3(b), respectively. In each figure, the waveform obtained at the point A represents the incident wave and the reflected wave, and the waveform at the point B corresponds to the transmitted wave. The incident waveform is located at around $14\,\mu$s, and the waveforms of the reflected and transmitted waves from the adhesive joint are at around $22\,\mu$s. It is noted that the scales of the horizontal axes in Figs. 3(a) and 3(b) are set to be different to show the waveforms clearly. In Fig. 3(a), the

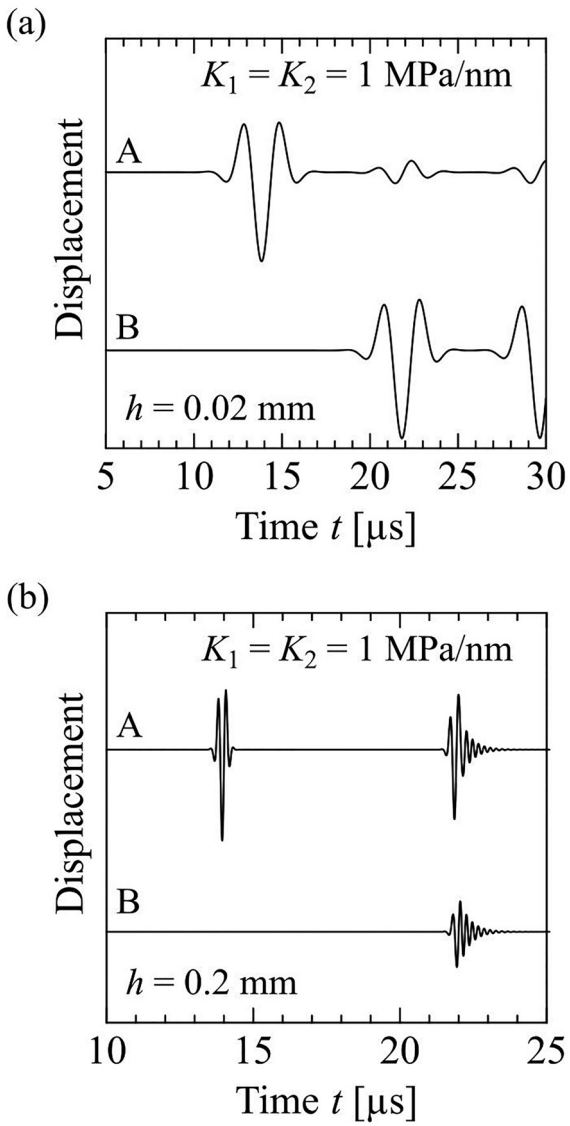

FIG. 3. Time histories of the incident and reflected waves at the point A and the transmitted wave at the point B in (a) case I and (b) case II at $K_1 = K_2 = 1$ MPa/nm, calculated by FEM.

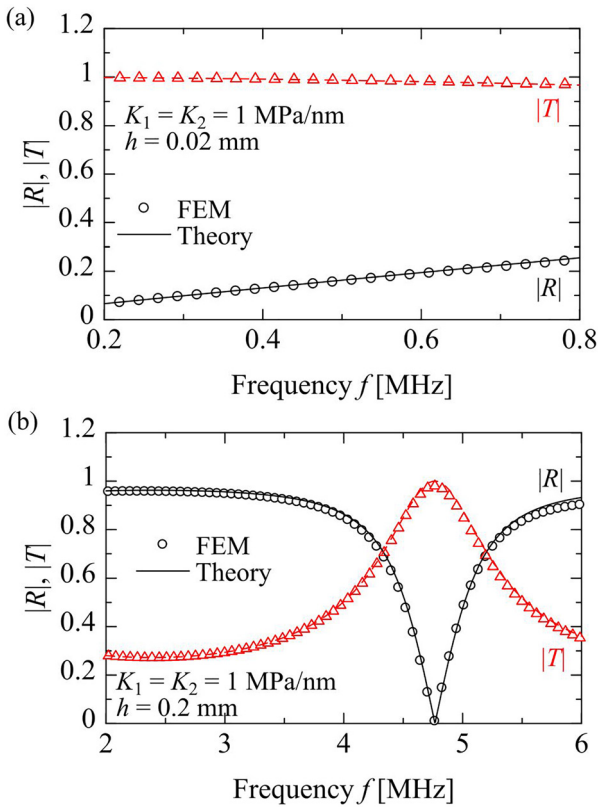

FIG. 4. (Color online) Comparison of the amplitude reflection and transmission coefficients obtained by FEM to the theoretical results: (a) case I and (b) case II at $K_1 = K_2 = 1$ MPa/nm.

reflected waves from the left and right edges of the adherends appear at around 30 μs, but hereafter these waves are not considered.

The amplitude spectra of the incident, reflected, and transmitted waves, denoted as $I(f)$, $P(f)$, and $Q(f)$, respectively, are obtained by spectral analysis using fast Fourier transform (FFT). The incident waveform is extracted by a rectangular window function of time range 10–18 μs, while the reflection and transmission waveforms are by a rectangular window of time range 18–25 μs. The amplitude reflection and transmission coefficients are calculated as functions of frequency

$$|R(f)| = \frac{P(f)}{I(f)}, \quad |T(f)| = \frac{Q(f)}{I(f)}, \tag{14}$$

respectively. The reflection and transmission coefficients obtained from the waveforms in Figs. 3(a) and 3(b) are shown in Figs. 4(a) and 4(b), respectively, together with the theoretical results obtained by Eq. (9) and $|T| = \sqrt{1 - |R|^2}$. As a result, the theoretical and numerical results are found to be in good agreement for both cases I and II, and the validity of the theoretical results is confirmed. The amplitude reflection and transmission coefficients vary monotonically with frequency in case I, while they show extremal behavior in case II. In Fig. 4(b), the reflection coefficient shows slight deviation above 5.5 MHz due to insufficient mesh sizes in the finite element simulation, but the local minimum (maximum) behavior of the reflection (transmission) coefficient is well reproduced by FEM. The dependence of the reflection and transmission coefficients on the frequency and the interfacial stiffnesses is further investigated in Sec. V.

V. RESULTS AND DISCUSSIONS

A. Case of a thin adhesive layer (case I)

The amplitude reflection and transmission coefficients are calculated from the theoretical relation of Eq. (9) for different interfacial stiffnesses K_1 and K_2 in case I. The obtained reflection and transmission coefficients at $K_2/K_1 = 1$ are shown for two different interfacial stiffnesses in Figs. 5(a) and 5(b), and the results for $K_2/K_1 < 1$ at a fixed interfacial stiffness $K_1 = 1$ MPa/nm are shown in Figs. 5(c) and 5(d), respectively. In all conditions, the reflection coefficient increases and the transmission coefficient decreases monotonically with increasing frequency. Furthermore, the interfacial stiffness K_S in the single-interface model is determined for each pair of K_1 and K_2 in Figs. 5(a)–5(d) from Eq. (11), and the reflection and

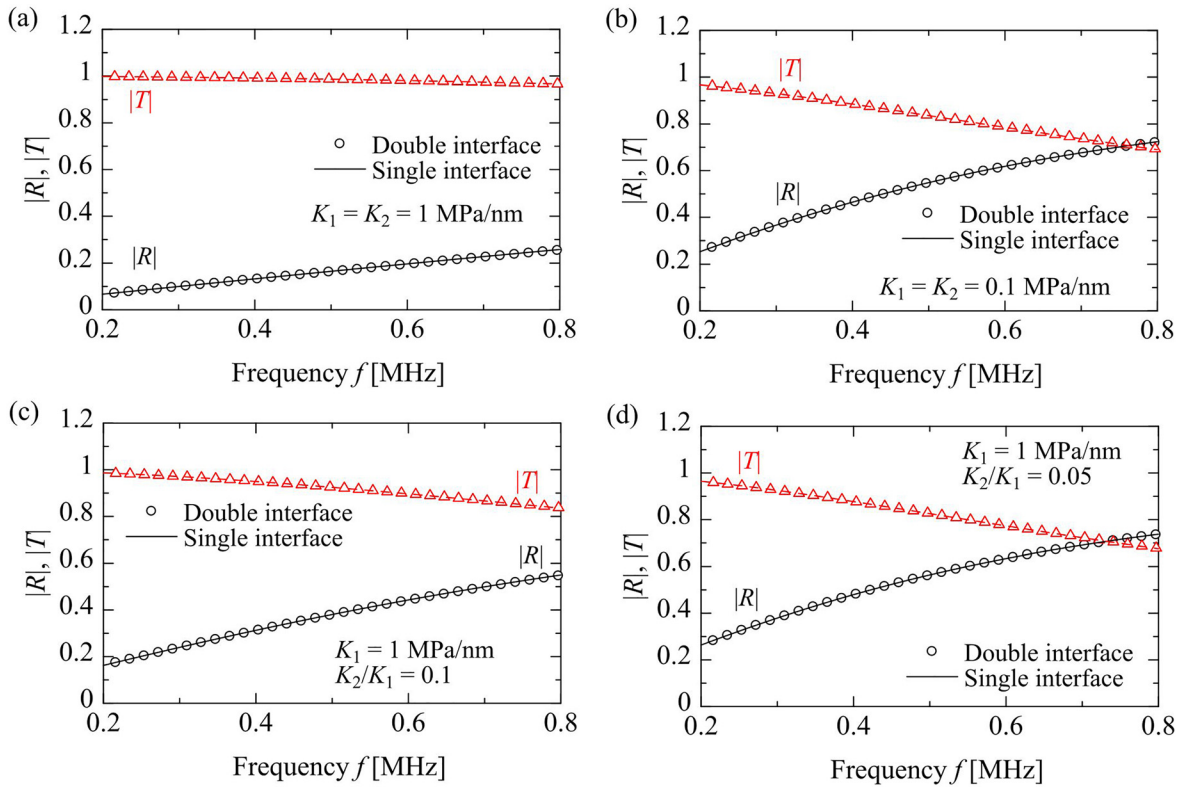

FIG. 5. (Color online) Comparison of the amplitude reflection and transmission coefficients in case I obtained from the double-interface model at (a) $K_1 = 1$ MPa/nm, $K_2/K_1 = 1$, (b) $K_1 = 0.1$ MPa/nm, $K_2/K_1 = 1$, (c) $K_1 = 1$ MPa/nm, $K_2/K_1 = 0.1$, and (d) $K_1 = 1$ MPa/nm, $K_2/K_1 = 0.05$, to the results for the single-interface model.

transmission coefficients in the single-interface model are calculated by Eq. (6). The obtained results are shown together in Figs. 5(a)–5(d). As a result, the reflection and transmission coefficients for the double-interface model are shown to be well reproduced by the single-interface model, whether the two interfacial stiffnesses K_1 and K_2 in the double-interface model are equal or not. This result indicates that the single-interface model can be applied to the adhesive joint in case I. In the actual measurement, if the interfacial stiffness in the single-interface model K_S is estimated from the measured reflection coefficient by Eq. (7) and the cohesive property $K_{AL} = \rho_A c_A^2/h$ is known *a priori*, the sum of the two interfacial compliances $1/K_1 + 1/K_2$ can be obtained from Eq. (11) without the direct use of the double-interface model.

When the sum of the two interfacial compliances is fixed at $1/K_1 + 1/K_2 = 2$ nm/MPa, the amplitude reflection and transmission coefficients for the double-interface model are calculated from Eq. (9) for different stiffness ratios K_2/K_1. The obtained results are shown in Fig. 6. In this figure, the cases of $K_2/K_1 = 0.05$ and $K_1/K_2 = 0.05$ represent the results for the interchange of the interfacial stiffnesses, which corresponds to the change of the incident surface in the adhesive joint. In other words, if the former case corresponds to the wave incidence from one adherend, the latter represents the incidence from the other adherend. In Fig. 6, the reflection and transmission coefficients for three different stiffness ratios K_2/K_1 show the same frequency dependences, respectively, even if the values of K_1 and K_2 are interchanged. Namely, the difference between the two interfacial stiffnesses K_1 and K_2 cannot be clarified from only the amplitude reflection and transmission coefficients in the frequency domain.

To seek difference among the three different interfacial conditions in Fig. 6, the transient behavior of the reflection and transmission at the adhesive joints is investigated by FEM. The reflection and transmission waveforms calculated at the two points A and B are shown in Fig. 7. In this figure, clear difference cannot be found among the waveforms for the three interfacial ratios if the sum of the interfacial compliances is fixed. Namely, when the adhesive thickness h is sufficiently small compared to the wavelength, not only the reflection and transmission coefficients in the frequency domain but also the temporal waveforms depend simply on

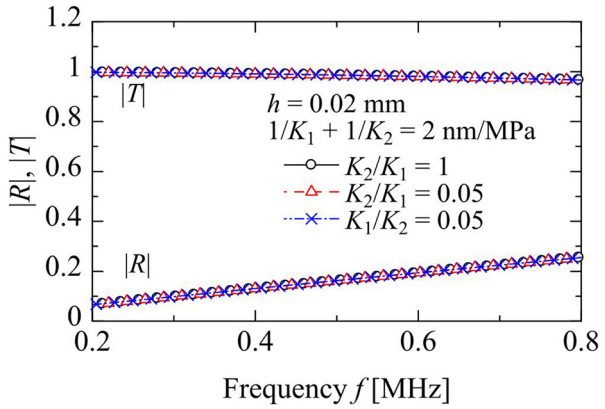

FIG. 6. (Color online) Variation of the amplitude reflection and transmission coefficients calculated for different stiffness ratios K_2/K_1 at $1/K_1 + 1/K_2 = 2$ nm/MPa with frequency, for the double-interface model in case I.

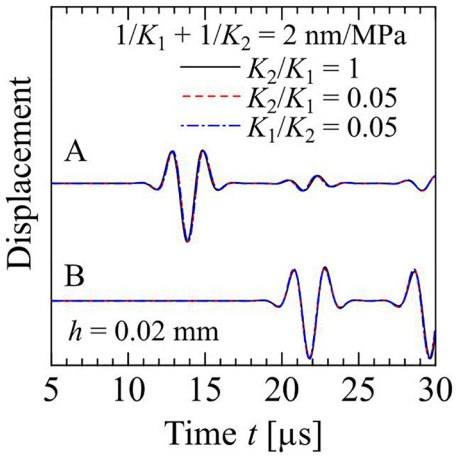

FIG. 7. (Color online) Time histories of the incident and reflected waves at the point A, and the transmitted wave at the point B, obtained by FEM for different stiffness ratios K_2/K_1 at $1/K_1 + 1/K_2 = 2$ nm/MPa.

the sum of the interfacial compliances $1/K_1 + 1/K_2$. Each interfacial compliance in the double-interface model cannot uniquely be determined from the reflection and transmission waveforms.

B. Case of a relatively thick adhesive layer (case II)

When the thickness of an adhesive layer is sufficiently thin compared to wavelength, the amplitude reflection coefficient increases monotonically with frequency as shown in Fig. 5. For a relatively thick adhesive layer, on the other hand, the reflection coefficient shows local minima due to the interference of waves multiply reflected in the interlayer.[3,35] In case II, the amplitude reflection coefficient at $K_1 = K_2 = 1$ MPa/nm is calculated from Eq. (9) and is shown in Fig. 8. Furthermore, the interfacial stiffness in the single-interface model K_S is calculated from Eq. (11), and the amplitude reflection coefficient obtained by Eq. (6) is shown together in Fig. 8. As a result, it is shown that the single-interface model cannot reproduce the local minimum behavior of the reflection coefficient in the double-interface model. The adhesive thickness h is not sufficiently small compared to the wavelength above around 1 MHz that the single-interface model cannot be related to the double-interface model by Eq. (6).

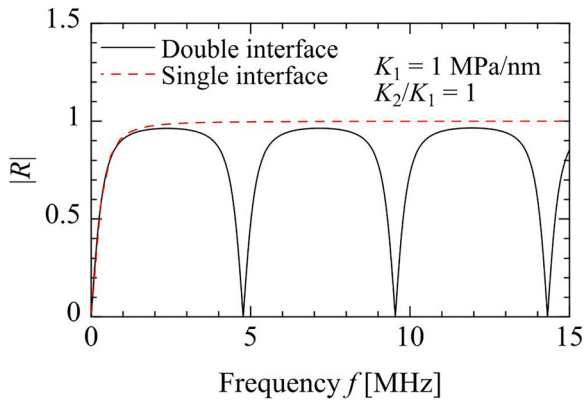

FIG. 8. (Color online) Comparison of the amplitude reflection coefficient calculated from the double-interface model at $K_1 = 1$ MPa/nm and $K_2/K_1 = 1$ to the results of the corresponding single-interface model.

The amplitude reflection coefficient in the double-interface model at $K_2/K_1 = 1$ is calculated for different interfacial stiffnesses K_1 from Eq. (9). The obtained results are shown in Fig. 9(a). The reflection coefficient for each interfacial stiffness becomes zero at three frequencies below 15 MHz, and the local minimum frequencies decrease as the interfacial stiffness decreases. This feature was reported in Ref. 35. For different stiffness ratios K_2/K_1, the amplitude reflection coefficient is calculated at a fixed interfacial stiffness $K_1 = 1$ MPa/nm, as shown in Fig. 9(b). As the stiffness ratio K_2/K_1 decreases, the local minimum frequencies are found to become low. This trend is analogous to the case of $K_2/K_1 = 1$ in Fig. 9(a) that the local minimum frequencies decrease with decreasing interfacial stiffness. On the other hand, the local minima seen in Fig. 9(b) increase with decreasing stiffness ratio K_2/K_1, which is not seen in the case of $K_2/K_1 = 1$. When the two interfacial stiffnesses K_1 and K_2 are identical, multiply reflected waves from the two interfaces are exactly canceled at certain frequencies due to the symmetry of the joint, so that the reflected wave amplitude becomes zero.[35] If the two interfacial stiffnesses are not equal, however, the symmetry breaks and the reflected wave cannot totally be canceled by the superposition of the

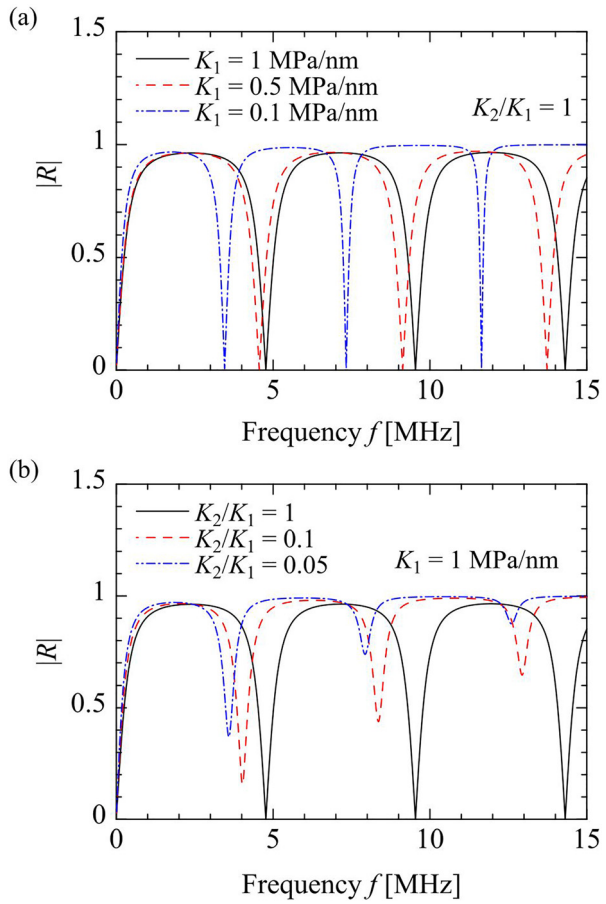

FIG. 9. (Color online) Effects of (a) the interfacial stiffness K_1 at a fixed stiffness ratio $K_2/K_1 = 1$ and (b) the stiffness ratio K_2/K_1 at a fixed interfacial stiffness $K_1 = 1$ MPa/nm on the frequency dependence of the amplitude reflection coefficient in the double-interface model.

multiply reflected waves from the interfaces. This non-zero local minimum behavior is characteristic of adhesive joints with one interfacial stiffness degraded compared to the other.

It is noted that if the values of K_1 and K_2 are interchanged, the frequency dependence of the amplitude reflection coefficient $|R|$ remains invariant as shown in Fig. 10. This feature appears because $|R|$ calculated from Eq. (9) has a symmetric form with respect to K_1 and K_2. Namely, it has no effect on the amplitude reflection coefficient in the frequency domain which of the two interfaces shows lower interfacial stiffness, similarly to the result of case I shown in Fig. 6.

To clarify the difference between the cases of $K_1/K_2 < 1$ and $K_1/K_2 > 1$, the reflection waveforms calculated by the time-domain FEM are further examined. Two conditions are considered here: (1) $K_1/K_2 = 0.05$, $K_2 = 1$ MPa/nm and (2) $K_2/K_1 = 0.05$, $K_1 = 1$ MPa/nm. These two situations correspond to the interchange of the interfacial stiffnesses, which represents the change of the incident surface in the adhesive joint. The obtained reflection waveforms are shown in Fig. 11. As a result, the reflection waveforms are found to show different features in the two conditions. The maximum displacement of the reflection waveform at $K_1/K_2 = 0.05$ is larger than that for $K_2/K_1 = 0.05$, and the latter shows a large-oscillation tail after 22 μs compared to the former. These features can also be illustrated in the time-frequency relations obtained by short-time Fourier transform (STFT), as shown in Figs. 12(a) and 12(b). At $K_1/K_2 = 0.05$, most of the reflected energy consists of the reflected wave at the left interface of interfacial stiffness K_1, which corresponds to relatively high wave amplitude at around 22 μs. In this case, the amplitude of the transmitted wave across the left interface becomes low compared to the result for $K_2/K_1 = 0.05$. Since the long-oscillation tails result from the multiple reflection in the adhesive layer, the temporal length of the reflection waveform for $K_1/K_2 = 0.05$ becomes relatively short. On the other hand, at $K_2/K_1 = 0.05$ the amplitude of the transmitted wave across the interface

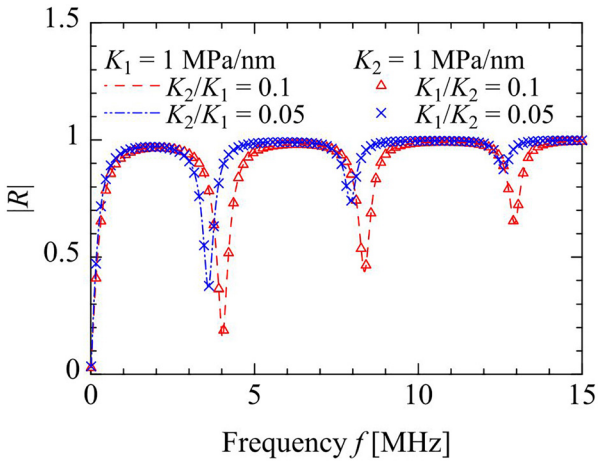

FIG. 10. (Color online) Effect of the interchange of the interfacial stiffnesses K_1 and K_2 on the frequency dependence of the amplitude reflection coefficient when $K_2/K_1 = 0.1$ and $K_2/K_1 = 0.05$ at $K_1 = 1$ MPa/nm, and when $K_1/K_2 = 0.1$ and $K_1/K_2 = 0.05$ at $K_2 = 1$ MPa/nm.

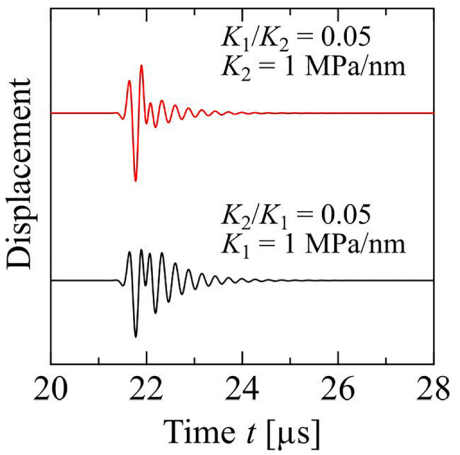

FIG. 11. (Color online) Reflection waveforms calculated at the point A for the double-interface model in case II at two different pairs of the interfacial stiffnesses, obtained by FEM.

of interfacial stiffness K_1 is relatively high, so that the long oscillation appears more clearly in the reflection waveform due to the multiple reflection. Namely, from the amplitude reflection coefficient it cannot be predicted which of the two interfaces shows lower interfacial stiffness, but that seems to be qualitatively distinguishable by comparing the two reflection waveforms acquired for the wave incidence from one adherend and the other. These results could be used for the detection of weak interfacial adhesion in adhesive joints by the reflection characteristics for the normal wave incidence, which remains as future work.

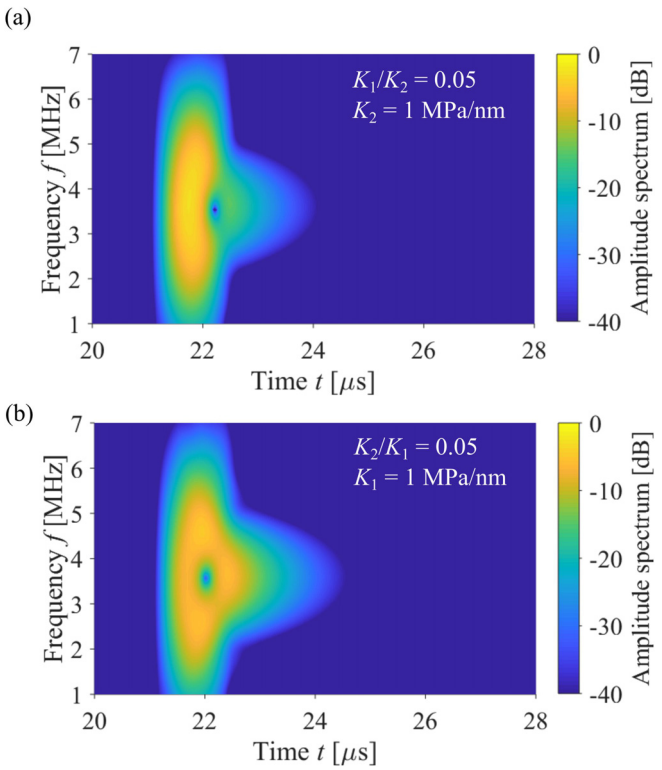

FIG. 12. (Color online) Time-frequency relations of the reflection waveforms for the double-interface model in case II at (a) $K_1/K_2 = 0.05$, $K_2 = 1$ MPa/nm and (b) $K_2/K_1 = 0.05$, $K_1 = 1$ MPa/nm.

VI. CONCLUSIONS

In this study, the effect of the interfacial stiffnesses on the reflection and transmission characteristics of normally incident ultrasonic waves at adhesively bonded joints has been investigated by one-dimensional wave propagation analysis. An adhesive joint has been modeled as a double-interface model, namely, a homogeneous layer coupled to adherends by two spring-type interfaces with different interfacial stiffnesses. When the thickness of the adhesive layer is sufficiently smaller than the wavelength, the double-interface model has been shown to correspond to a single spring-type interface model, whose interfacial stiffness is expressed by the cohesive and adhesive properties of the bonded joint. Even if the values of the two interfacial stiffnesses in the double-interface model have been replaced each other, the reflection and transmission behavior has been invariant in the time domain as well as in the frequency domain. On the other hand, when the adhesive thickness is comparable to the wavelength, the reflection coefficient has shown the local minima at certain frequencies, which are not reproduced by the single-interface model. As one interfacial stiffness decreases, the local minimum frequencies have become low and the local minima have increased. The frequency dependence of the reflection coefficient has remained invariant if the values of the two interfacial stiffnesses are interchanged. However, the reflection waveform has shown different features including the waveform amplitude and the oscillation tail due to the contrast between the two interfacial stiffnesses.

ACKNOWLEDGMENTS

This study has been supported by Grant-in-Aids for Scientific Research (KAKENHI) Grant Nos. JP17H07254 and JP18K13663 from Japan Society for the Promotion of Science (JSPS).

[1]C. C. H. Guyott, P. Cawley, and R. D. Adams, "The non-destructive testing of adhesively bonded structure: A review," J. Adhes. **20**, 129–159 (1986).
[2]R. D. Adams and P. Cawley, "A review of defect types and nondestructive testing techniques for composites and bonded joints," NDT Int. **21**, 208–222 (1988).
[3]C. C. H. Guyott and P. Cawley, "Evaluation of the cohesive properties of adhesive joints using ultrasonic spectroscopy," NDT Int. **21**, 233–240 (1988).
[4]P. N. Dewen and P. Cawley, "Ultrasonic determination of the cohesive properties of bonded joints by measurement of reflection coefficient and bondline transit time," J. Adhes. **40**, 207–227 (1993).
[5]L. M. Brekhovskikh, *Waves in Layered Media*, 2nd ed. (Academic, New York, 1976), pp. 15–23.
[6]F. H. Chang, P. L. Flynn, D. E. Gordon, and J. R. Bell, "Principles and application of ultrasonic spectroscopy in NDE of adhesive bonds," IEEE Trans. Sonics Ultrason. **23**, 334–338 (1976).
[7]P. B. Nagy and L. Adler, "Nondestructive evaluation of adhesive joints by guided waves," J. Appl. Phys. **66**, 4658–4663 (1989).
[8]S. I. Rokhlin and Y. J. Wang, "Analysis of boundary conditions for elastic wave interaction with an interface between two solids," J. Acoust. Soc. Am. **89**, 503–515 (1991).
[9]S. I. Rokhlin and W. Huang, "Ultrasonic wave interaction with a thin anisotropic layer between two anisotropic solids: Exact and asymptotic-boundary-condition methods," J. Acoust. Soc. Am. **92**, 1729–1742(1992).
[10]A. I. Lavrentyev and S. I. Rokhlin, "Determination of elastic moduli, density, attenuation, and thickness of a layer using ultrasonic spectroscopy at two angles," J. Acoust. Soc. Am. **102**, 3467–3477 (1997).
[11]M. J. S. Lowe, R. E. Challis, and C. W. Chan, "The transmission of Lamb waves across adhesively bonded lap joints," J. Acoust. Soc. Am. **107**, 1333–1345 (2000).
[12]R. Seifried, L. J. Jacobs, and J. Qu, "Propagation of guided waves in adhesive bonded components," NDT E Int. **35**, 317–328 (2002).
[13]J. M. Allin, P. Cawley, and M. J. S. Lowe, "Adhesive disbond detection of automotive components using first mode ultrasonic resonance," NDT E Int. **36**, 503–514 (2003).
[14]M. V. Predoi and M. Rousseau, "Lamb waves propagation in elastic plane layers with a joint strip," Ultrasonics **43**, 551–559 (2005).
[15]B. Ren and C. J. Lissenden, "Ultrasonic guided wave inspection of adhesive bonds between composite laminates," Int. J. Adhes. Adhes. **45**, 59–68 (2013).
[16]J. P. Jones and J. S. Whittier, "Waves at a flexibly bonded interface," J. Appl. Mech. **34**, 905–909 (1967).
[17]H. G. Tattersall, "The ultrasonic pulse-echo technique as applied to adhesion testing," J. Phys. D. Appl. Phys. **6**, 819–832 (1973).
[18]M. Schoenberg, "Elastic wave behavior across linear slip interfaces," J. Acoust. Soc. Am. **68**, 1516–1521 (1980).
[19]J. M. Baik and R. B. Thompson, "Ultrasonic scattering from imperfect interfaces: A quasi-static model," J. Nondestruct. Eval. **4**, 177–196 (1984).
[20]A. Pilarski and J. L. Rose, "Ultrasonic oblique incidence for improved sensitivity in interface weakness determination," NDT Int. **21**, 241–246 (1988).
[21]P. B. Nagy, "Ultrasonic classification of imperfect interfaces," J. Nondestruct. Eval. **11**, 127–139 (1992).
[22]P. Fraisse, F. Schmit, and A. Zarembowitch, "Ultrasonic inspection of very thin adhesive layers," J. Appl. Phys. **72**, 3264–3271 (1992).
[23]W. Wang and S. I. Rokhlin, "Evaluation of interfacial properties in adhesive joints of aluminum alloys using angle-beam ultrasonic spectroscopy," J. Adhes. Sci. Technol. **5**, 647–666 (1991).
[24]A. I. Lavrentyev and S. I. Rokhlin, "Models for ultrasonic characterization of environmental degradation of interfaces in adhesive joints," J. Appl. Phys. **76**, 4643–4650 (1994).
[25]M. J. S. Lowe, "Matrix techniques for modeling ultrasonic waves in multilayered media," IEEE Trans. Ultrason. Ferroelectr. Freq. Control **42**, 525–542 (1995).
[26]A. Pilarski, J. L. Rose, and K. Balasubramaniam, "The angular and frequency characteristics of reflectivity from a solid layer embedded between two solids with imperfect boundary conditions," J. Acoust. Soc. Am. **87**, 532–542 (1990).
[27]J. L. Rose, *Ultrasonic Waves in Solid Media* (Cambridge University Press, Cambridge, 1999), pp. 60–80.
[28]A. Baltazar, L. Wang, B. Xie, and S. I. Rokhlin, "Inverse ultrasonic determination of imperfect interfaces and bulk properties of a layer between two solids," J. Acoust. Soc. Am. **114**, 1424–1434 (2003).
[29]B. Hosten and M. Castaings, "Surface impedance matrices to model the propagation in multilayered media," Ultrasonics **41**, 501–507 (2003).
[30]R. L. Vijaya Kumar, M. R. Bhat, and C. R. L. Murthy, "Some studies on evaluation of degradation in composite adhesive joints using ultrasonic techniques," Ultrasonics **53**, 1150–1162 (2013).
[31]M. Castaings, "SH ultrasonic guided waves for the evaluation of interfacial adhesion," Ultrasonics **54**, 1760–1775 (2014).
[32]S. Mezil, F. Bruno, S. Raetz, J. Laurent, D. Royer, and C. Prada, "Investigation of interfacial stiffnesses of a tri-layer using Zero-Group Velocity Lamb modes," J. Acoust. Soc. Am. **138**, 3202–3209 (2015).
[33]N. Mori and S. Biwa, "Transmission of Lamb waves and resonance at an adhesive butt joint of plates," Ultrasonics **72**, 80–88 (2016).
[34]H. A. Haldren, D. F. Perey, W. T. Yost, K. E. Cramer, and M. C. Gupta, "Swept-frequency ultrasonic phase evaluation of adhesive bonding in tri-layer structures," J. Acoust. Soc. Am. **145**, 1609–1618 (2019).
[35]A. I. Lavrentyev and S. I. Rokhlin, "Ultrasonic spectroscopy of imperfect contact interfaces between a layer and two solids," J. Acoust. Soc. Am. **103**, 657–664 (1998).
[36]B. W. Drinkwater, R. S. Dwyer-Joyce, and P. Cawley, "A study of the interaction between ultrasound and a partially contacting solid-solid interface," Proc. R. Soc. A: Math. Phys. Eng. Sci. **452**, 2613–2628 (1996).
[37]A. Balvantín, A. Baltazar, and J. I. Aranda-Sanchez, "A study of guided wave propagation on a plate between two solid bodies with imperfect boundary conditions," Int. J. Mech. Sci. **63**, 66–73 (2012).

[38]N. Mori and S. Biwa, "Transmission characteristics of the S0 and A0 Lamb waves at contacting edges of plates," Ultrasonics **81**, 93–99 (2017).
[39]H. Lekesiza, N. Katsube, S. I. Rokhlin, and R. R. Seghic, "Effective spring stiffness for a periodic array of interacting coplanar penny-shaped cracks at an interface between two dissimilar isotropic materials," Int. J. Solid Struct. **50**, 2817–2828 (2013).
[40]M. V. Golub and O. V. Doroshenko, "Effective spring boundary conditions for modelling wave transmission through a composite with a random distribution of interface circular cracks," Int. J. Solid Struct. **165**, 115–126 (2019).
[41]M. V. Golub and A. Boström, "Interface damage modeled by spring boundary conditions for in-plane elastic waves," Wave Motion **48**, 105–115 (2011).